INTERNATIONAL JOURNAL FOR NUMERICAL AND ANALYTICAL METHODS IN GEOMECHANICS, VOL. 21, 255–275 (1997)

DYNAMIC RESPONSE OF INTACT PILES TO IMPULSE LOADS

SHUTAO T. LIAO* AND JOSE M. ROESSET†

*Department of Civil Engineering, Chung-Hua Polytechnic Institute, Hsin-Chu 30067, Taiwan
†Department of Civil Engineering, The University of Texas at Austin, Austin, TX 78712-1076, U.S.A.

SUMMARY

The objective of this work was to evaluate the theoretical capabilities of the non-destructive impact–response method in estimating the length and cross-sectional area of intact piles. Three-dimensional (3-D) axisymmetric finite element models were developed to simulate the testing. The results obtained were compared to one-dimensional solutions to evaluate the importance of 3-D effects. Extensive parametric studies were then performed on piles without defects. In each parametric study, the results from the direct use of time histories of displacements or velocities, the mobility function and the Fourier transform of the recorded displacements (impact-echo method) were compared in order to assess their relative advantages and disadvantages. The effects of the relative stiffness of the surrounding soil to that of the pile and of the embedment depth were also investigated for all three methods. In a companion paper the use of these procedures to detect defects such as bulbs (increases in the cross-sectional area of the pile) or necks (decreases in area) is studied. © 1997 by John Wiley & Sons, Ltd. Int. j. numer. anal. methods geomech., vol. 21, 255–275 (1997)

(No. of Figures: 27 No. of Tables: 2 No. of Refs: 32)

Key words: intact piles; dynamic response; non-destructive impact-response method

1. INTRODUCTION

The importance of assessing the construction quality of a pile foundation has long been recognized. Over 30 yrs ago there were already a number of alternative techniques used to evaluate the integrity of piles as summarized by Whitaker.[1] Methods based on vibration measurements, of particular interest in the context of this paper and shown schematically in Figure 1, were proposed by Paquet[2] for concrete piers and then by Briard.[3] Davis and Dunn[4] suggested the use of steady-state harmonic excitation at a specified set of frequencies and introduced the concept of mechanical admittance (or mobility function) as a means to determine the length and cross-sectional area of a pile. The mobility is the ratio of the amplitude of the response velocity at the pile head to the amplitude of the harmonic excitation (applied also at the top) as a function of frequency. Davis and Robertson[5] used this same procedure to determine the pile head stiffness and Higgs[6] suggested a modification applying an impact load instead of steady-state harmonic excitations. The mobility function is then computed by finding the Fourier transforms of the response velocity and the input load and dividing the former by the latter. This

*Associate Professor
†Joe J. King Chair in Engineering

CCC 0363–9061/97/040255–21$17.50

Received 1 March 1996
Revised 20 August 1996

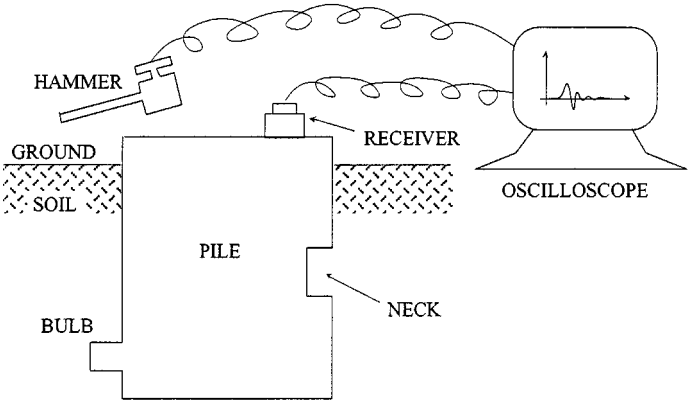

Figure 1. Impact-response test of piles

alternative, defined as the shock method, is essentially the same as the impact response method commonly used at present, where the Fast Fourier Transform is employed. Stain[7,8] summarized the procedure and reported the results of field tests. Lin *et al.*[9] suggested another alternative, referred to as the impact-echo method, using the amplitude Fourier spectrum of the displacement record at the pile head instead of the mobility function. This method has been used successfully to locate voids or other flaws in concrete elements.[10–22] Schellingerhout[23] used one-dimensional wave theory and the concept of impedance change to quantify defects in a column and concluded that the wavelength of the shock wave had an important effect on the resolution of the results.

Most of the analytical or numerical work conducted to interpret the results of vibratory pile tests have used 1-D models. However, 2-D and 3-D finite element models were used by Lin *et al.*[9] who conducted analyses of piles subjected to impact loads with the computer codes DYNA2D[24] and DYNA3D.[25] Further comparisons of the results predicted by 1-D, 2-D and 3-D models have been conducted by Liao[26] using specially developed computer programs.

The objective of this work was to compare the following methods: (1) the direct use of time histories of displacements or velocities, (2) the mobility function, and (3) the Fourier transform of the recorded displacements (impact-echo method) as means to determine the length and cross-sectional area of intact piles. The relative advantages and disadvantages of the methods were then determined. The effects of the relative stiffness of the surrounding soil to that of the pile and of the embedment depth are also investigated for all three methods. In a companion paper the use of these procedures to detect defects such as bulbs (increases in the cross-sectional area of the pile) or necks (decreases in area) is studied.

2. PROBLEM DEFINITION

2.1. Geometry

Consider a pile partially or fully embedded in soil, as shown in Figure 2(a). The pile system consists of a column, which is assumed to be made of concrete, and the soil. The pile has a circular cross-sectional area with a radius r_p. The lengths of the pile above and below the ground are denoted by H_T and H_B, respectively such that the total length, $L = H_T + H_B$. An external impact is applied at the top of the pile over a circular area with a radius r_L. An example is shown in

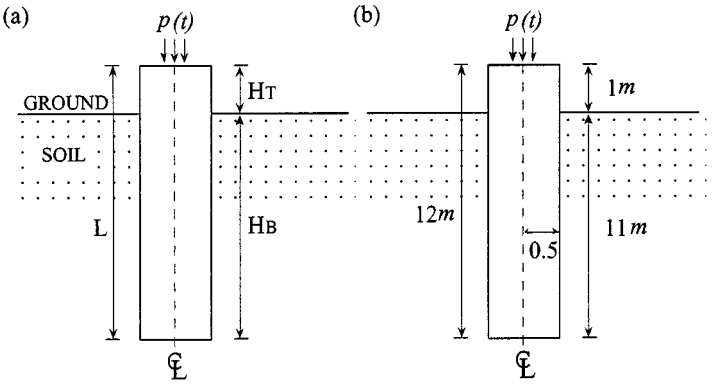

Figure 2. (a) Definition of pile problem and (b) an example

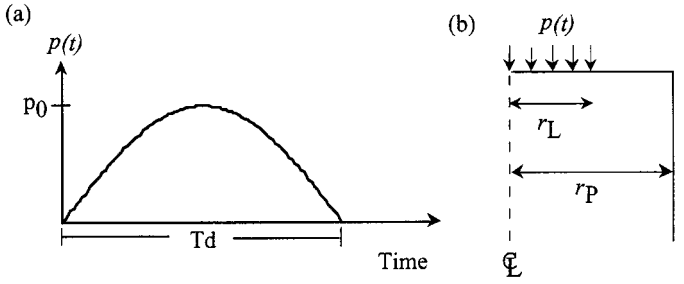

Figure 3. (a) Sinusoidal impact and (b) the loaded area

Figure 2(b) with $r_P = 0{\cdot}5$, $r_L = 0{\cdot}0254$, $L = 12$, $H_T = 1$, $H_B = 11$ m. The receiver is placed 0·4 m away from the centre on the top surface of the pile.

2.2. Loading conditions

The loading pressure $p(t)$ used in this work was defined as a function of time by

$$p(t) = p_0 \sin \bar{\omega} t \quad \text{when} \quad 0 \leqslant t \leqslant T_d \tag{1}$$

and $p(t) = 0$ for $t > T_d$ where $\bar{\omega} = \pi / T_d$. This represents a sinusoidal impact of half a cycle duration with a period of $2T_d$ s, as shown in Figure 3. In this work, $T_d = 1{\cdot}5 \times 10^{-3}$ s and $p_0 = 15570$ N/m^2. The effect of the duration of the impact T_d was investigated by Liao.[26]

2.3. Material properties

The material properties used in most of the studies are provided in Table I for the pile and soil. In this table, E is Young's modulus, ρ is the mass density, v is Poisson's ratio, γ is the unit weight and G is the shear modulus. The subscript c stands for concrete and the subscript s for soil. These data have been selected to be representative of practical situations. The propagation velocities corresponding to the material properties used are also listed in the table. These theoretical wave velocities V_p, V_s, and V_R are referred to as the P-, S- and Rayleigh wave velocities, respectively,

Table I. Concrete and soil properties and wave velocities (E, G in N/m^2, ρ in Kg/m^3, γ in N/m^3 and velocity in m/s)

	Concrete				Soil		
E_c	$3{\cdot}31 \times 10^{10}$	V_{rod}	3790	E_s	$1{\cdot}8 \times 10^8$	V_{rod}	310
ρ_c	2300	V_p	4000	ρ_s	1924	V_p	450
ν_c	0·2	V_s	2450	ν_s	0·4	V_s	180
γ_c	22540	V_R	2230	γ_s	18850	V_R	170
G_c	$1{\cdot}38 \times 10^{10}$			G_s	$6{\cdot}43 \times 10^7$		

and V_{rod} is the 1-D longitudinal wave propagation velocity in a rod. They are given by

$$V_p = \sqrt{\left[\frac{E(1-\nu)}{(1+\nu)(1-2\nu)\rho}\right]} \tag{2}$$

$$V_s = \sqrt{\left(\frac{G}{\rho}\right)} = \sqrt{\left(\frac{E}{2(1+\nu)\rho}\right)} \tag{3}$$

$$V_{rod} = \sqrt{\left(\frac{E}{\rho}\right)} \tag{4}$$

$$V_R = \alpha \times V_s \tag{5}$$

where α is a function of Poisson's ratio.[27] For $\nu = 0{\cdot}2$ and $0{\cdot}4$, $\alpha = 0{\cdot}9111$ and $0{\cdot}9423$, respectively.

2.4. *One-dimensional model*

The 1-D model used to simulate the solutions normally used in practice consisted of standard linear elements under axial deformation, with a linear variation of displacements. To simulate the effect of the soil on the lateral surface of the pile, distributed springs with elastic stiffness k_v and dashpots with damping coefficient c_v were applied to each segment below the ground surface as shown in Figure 4. The soil at the base of the pile was modelled using a spring with elastic constant K_v and a dashpot with damping coefficient C_v. c_v and C_v are intended to represent the radiation (or geometric) damping. The internal damping in the pile and the soil are assumed to be negligibly small under very small amplitude non-destructive loading. Consistent foundation matrices (including both the springs and dashpots) were developed for these elements. The values of k_v, c_v, K_v, and C_v per unit length of pile were determined through the following equations.[28–32,26]

$$k_v = 2{\cdot}3\ G_s\ (\mathrm{N/m^2}) \tag{6}$$

$$c_v = 2\pi\rho_s V_s r_P\ (\mathrm{Kg/m-s}) \tag{7}$$

$$K_v = 4G_s r_P/(1-\nu_s)\ (\mathrm{N/m}) \tag{8}$$

$$C_v = 0{\cdot}85\ K_v r_P/V_s\ (N\ \mathrm{m/s}) \tag{9}$$

The above equations were derived assuming a rigid disk in an elastic plane. The values of K_v and C_v correspond to a circular footing resting on top of the soil, an assumption which is not strictly correct for the base of a pile. However the error introduced by this simplifying assumption is small. Lumped masses were used at each point.

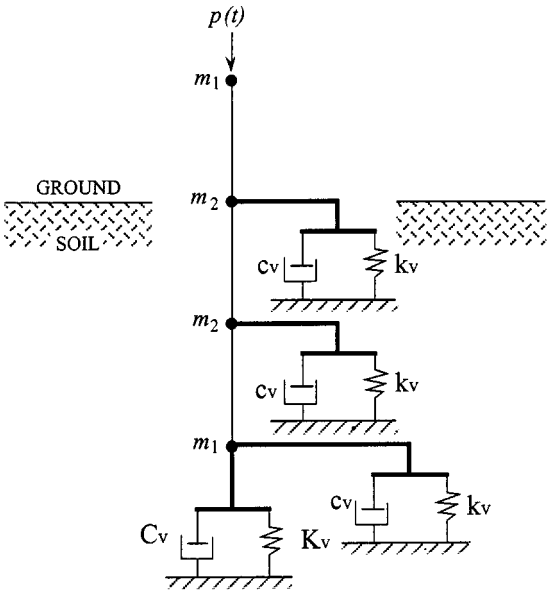

Figure 4. One-dimensional finite element model for piles partially embedded in soil

2.5. *Three-dimensional axisymmetric model*

Four-node, isoparametric, axisymmetric finite elements were used to model the pile and the surrounding soil in the 3-D analyses as shown in Figure 5. In this model the cross-section of the pile is always assumed to be circular. The complete domain of the problem can be obtained by rotating this figure about the centreline of the pile. The mesh size of the pile is denoted by $\{N_h, N_v\}$ where N_h and N_v represent the total number of finite elements in the radial and vertical directions, respectively. The domain involved in the analysis must be large enough to avoid stress waves reflected at the far boundaries coming back to the location of the receiver within the time span of interest. The central difference scheme was adopted to carry out the integration of the equations of motion for these finite element models.[26]

3. MECHANICAL ADMITTANCE AND IMPACT-ECHO METHODS

3.1. *Mechanical admittance method*

The mechanical admittance of a pile is obtained by applying an impact force at the top of the pile, recording the time histories of the impact and the corresponding velocity response, transforming them into the frequency domain using the Fast Fourier Transform (FFT), and computing the ratio

$$M_a = |V_0/\bar{p}_0| \tag{10}$$

where V_0 and $\bar{p}_0$ are the complex values of the Fourier transforms of the particle velocity and the impact force at each specific frequency. The operator $|\ |$ represents the modulus. An example of the mechanical admittance of a pile is illustrated in Figure 6.

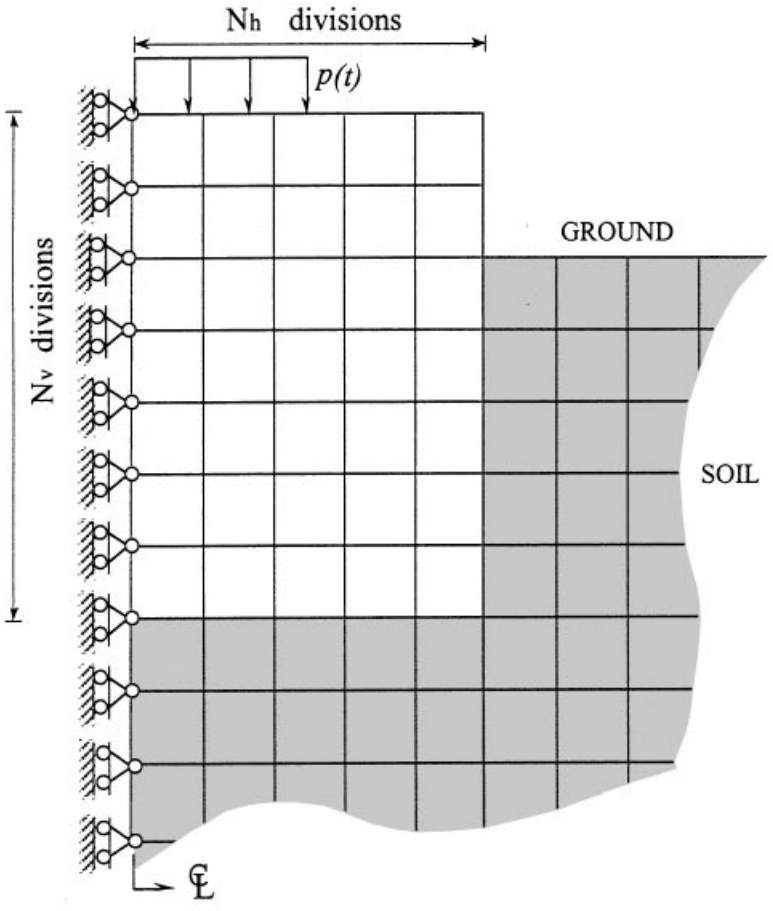

Figure 5. Three-dimensional finite element model for piles

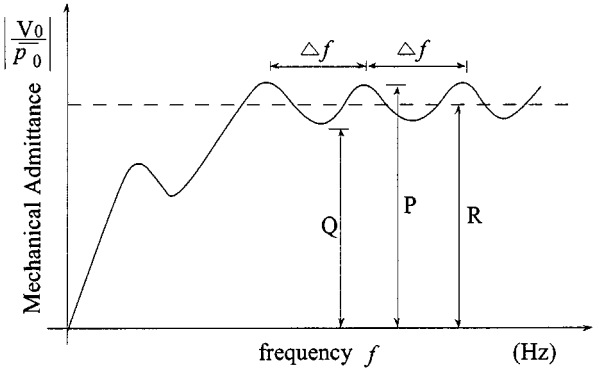

Figure 6. Mechanical admittance response curve of a pile (after Ref. 4)

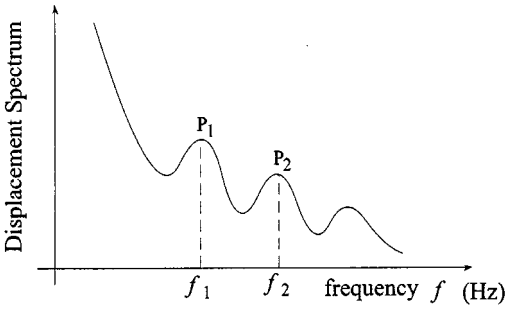

Figure 7. Displacement spectrum[9] of a pile

In the figure, there is usually a linear portion at low frequencies followed by a transition zone and a steady-state response region. The following notation and definitions are used

(1) P is the maximum value (or the peak) and Q is the minimum value (or the trough) of the response curve in the steady-state region.
(2) Δf is the frequency interval between two consecutive peaks (or troughs) of the response curve in the steady-state region.

Some useful relationships[4] between the parameters of the pile can then be established through the following equations:

$$R = \sqrt{PQ}\ (\text{m/s N}) \tag{11}$$

$$L = \frac{V_{\text{rod}}}{2\Delta f}\ (\text{m}) \tag{12}$$

$$A_{\text{c}} = \frac{1}{R\rho_{\text{c}}V_{\text{rod}}}\ (\text{m}^2) \tag{13}$$

where R is the geometric mean of P and Q, A_{c} is the cross-sectional area of the pile, ρ_{c} its mass density, and V_{rod} is the rod wave velocity in the pile.

The total length and the cross-sectional area of the pile can thus be determined through equations (12) and (13), respectively.

In the impact-echo method the Fourier transform of the displacement is used instead of the mobility curve. The displacement spectrum will exhibit a series of peaks associated with the natural frequencies of the pile and the time it takes the longitudinal waves to travel from the point of impact to the pile bottom and reflect back to the top. For a normal floating pile if the first peak occurs at a frequency f_1 the pile length is

$$L = V_{\text{rod}}/2f_1 \tag{14}$$

where V_{rod} is again the rod wave velocity in the pile. Alternatively one can use equation (12) above to predict the length from the frequency difference between successive peaks. Figure 7 shows a typical displacement spectrum.

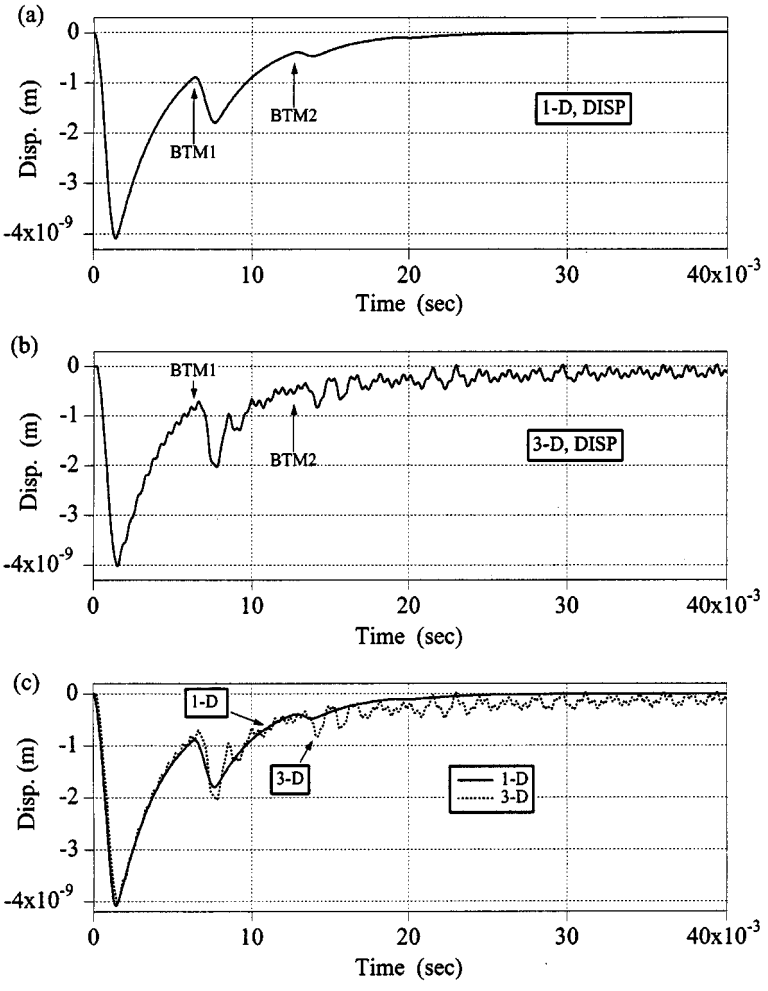

Figure 8. Displacement at top of pile with $H_T = 1$, $H_B = 11$, using (a) 1-D ($N_v - 120$), (b) 3-D ($\{N_h, N_v\} = \{5, 120\}$) and (c) 1-D and 3-D models

4. RESULTS AND DISCUSSION

4.1. *Effects of models*

Consider the pile of Figure 2(b), embedded 11 meters in the soil and with 1 meter above ground. The displacement time histories obtained with the 1-D and 3-D finite element models are shown in Figures 8(a) and 8(b), and they are plotted together in Figure 8(c). It can be seen that the results from the two models are very close. However, the 3-D results exhibit some high frequency fluctuations over the entire duration due in some part to the finite element discretization but primarily due to the combined effects of reflections and refractions of the waves from the lateral boundaries and interfaces. To evaluate the wave arrival times in the 1-D model let t_b denote the theoretical times for the longitudinal wave to travel back from the bottom of the pile. Then

$$t_b = 24/V_{rod} = 24/3790 = 6{\cdot}3 \times 10^{-3}\ \text{s}$$

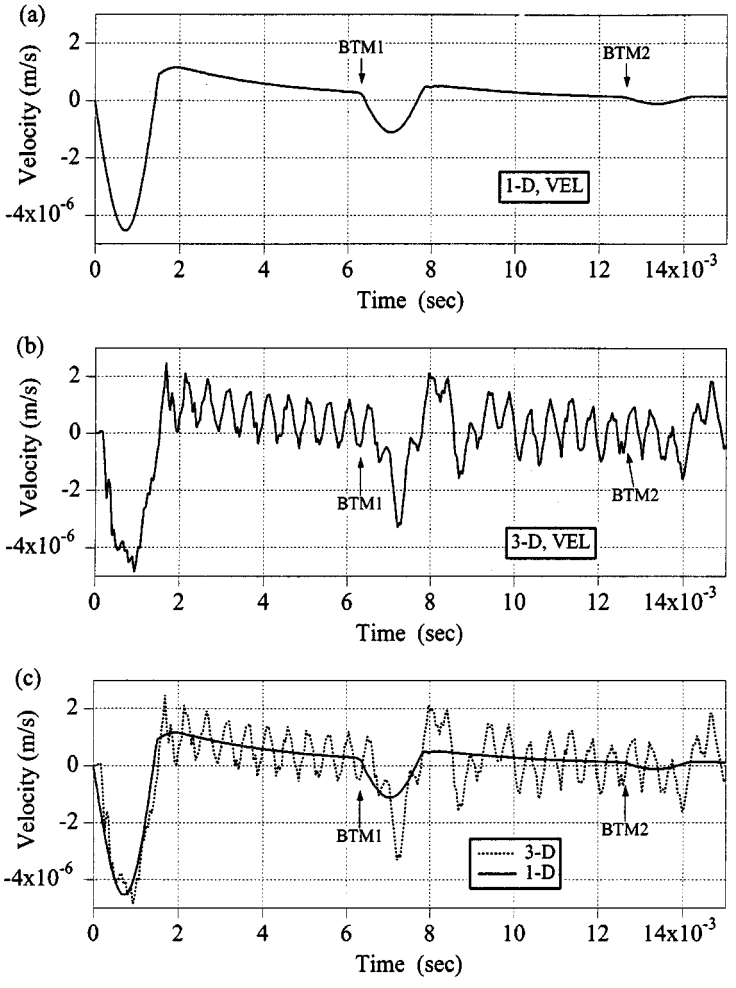

Figure 9. Velocity at top of pile wih $H_T = 1$, $H_B = 11$, using (a) 1-D, (b) 3-D, and (c) 1-D and 3-D models

The arrival times are marked in the figure with 'BTMn' where n indicates the sequence number of the arrivals. It can be seen that the theoretical times agree well with the finite element results.

The velocity and acceleration time histories corresponding to the displacements shown in Figure 8 are presented in Figures 9 and 10, respectively, over the smaller time range $0 \leqslant t \leqslant 15 \times 10^{-3}$. It is first observed that the wave arrival times are as easy or easier to identify from the 1-D velocity and acceleration records (Figures 9(a) and 10(a)) as from the displacement record. The duration of the excursion corresponding to the arrival of each longitudinal wave is equal to the duration of the applied impact, $T_d = 1{\cdot}5 \times 10^{-3}$ s. The situation is more complicated for the 3-D model where the large fluctuations tend to obscure the picture. Identification of the arrival times is difficult for the velocity record corresponding to the 3-D model and almost impossible from the acceleration record.

In practice the high frequencies would be automatically filtered out using appropriate band pass filters. To simulate the effect of this filtering, the records in the time domain were

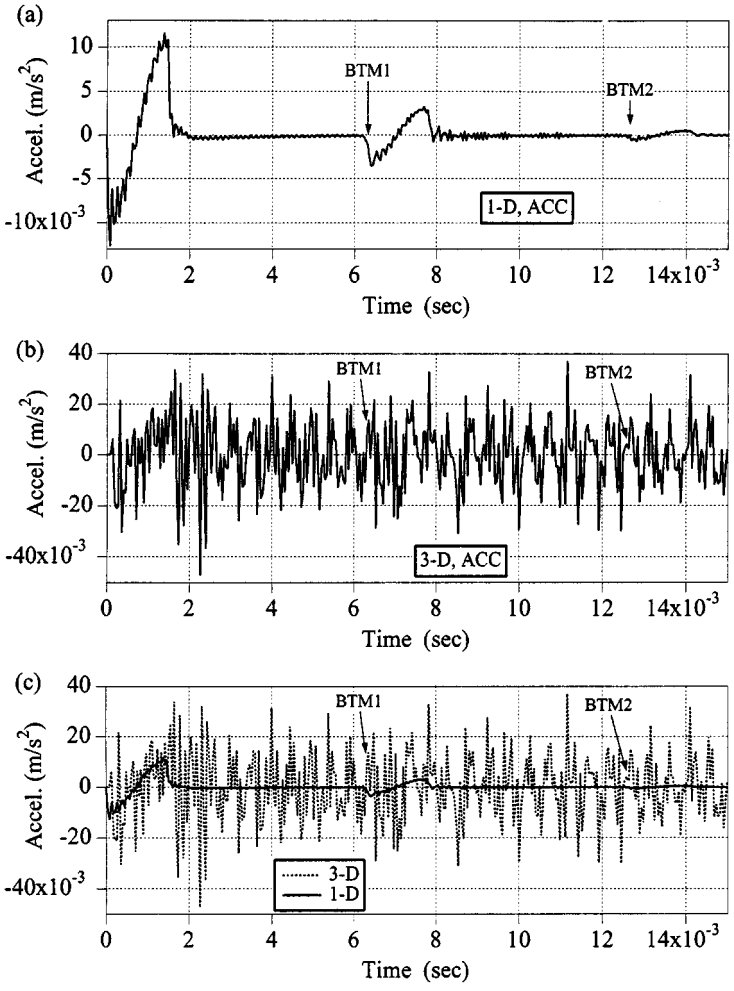

Figure 10. Acceleration at top of pile with $H_T = 1$, $H_B = 11$, using (a) 1-D, (b) 3-D, and (c) 1-D and 3-D models

transformed into the frequency domain using the Fast Fourier transform (FFT). The components higher than a specific frequency f_H were then filtered out and the new time records were recovered using the inverse FFT. The filtered displacement, velocity, and acceleration records are shown in Figures 11(a)–11(c) with $f_H = 500$ or 1000 Hz. The advantage of using filters for the 3-D results is very noticeable, especially for the acceleration records where analysing the results was almost impossible without filtering. However, f_H cannot be taken too low because some important signals might be filtered out.

4.2. Effect of pile-to-soil stiffness ratio

To investigate the effect of the relative stiffness of the pile and the soil, the material properties of the pile were kept the same but the Young's modulus of the soil E_s was varied. Values of the pile-to-soil stiffness ratio, k_E (ratio of the corresponding Young's moduli), of 184, 50, 10, and 1 were investigated. Only the 3-D axisymmetric model was used to carry out these studies.

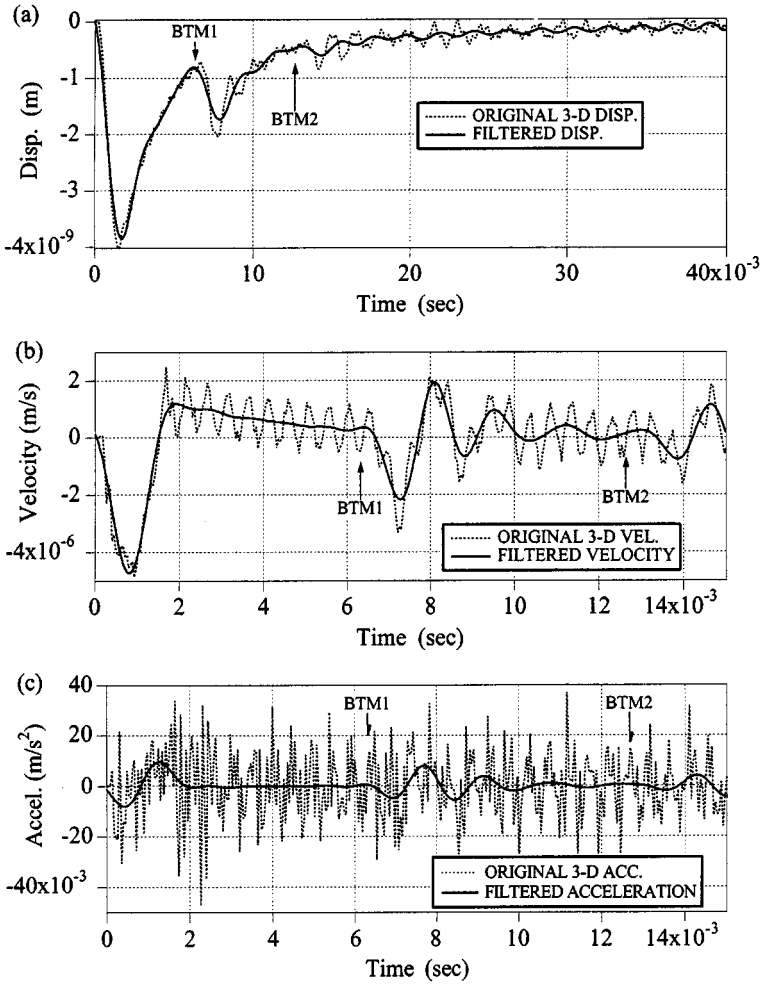

Figure 11. Original and filtered (a) displacement ($f_H = 500$), (b) velocity ($f_H = 1000$), and (c) acceleration ($f_H = 1000$ Hz) at top of pile with $H_T = 1$, $H_B = 11$, using 3-D models

The displacement time histories for the pile of Figure 2(b) with $k_E = 184$, 50, 10, and 1 are presented in Figure 12. It can be seen that the maximum displacement at the top of the pile decreases as the stiffness of the soil increases. It is also seen that the energy is dissipated into the soil very rapidly for all cases. The dissipation rate increases with the stiffness of the soil, and the pile system with $k_E = 1$ requires the smallest time period to return to its initial status at rest. The reflection signals ('BTM1') are identifiable for the soft soil cases with $k_E = 184$ and 50, but not for hard soil cases with $k_E = 10$ and 1.

The corresponding velocities are presented in Figures 13(a)–13(c). The filtered solutions with $f_H = 1000$ Hz are also plotted in the figures. It is easy to characterize the arrival of the first reflection from the filtered velocities for soft soil with $k_E = 184$ and 50 but it is impossible to do so for $k_E = 10$. The solution for $k_E = 1$ is not shown because it does not provide any new insights.

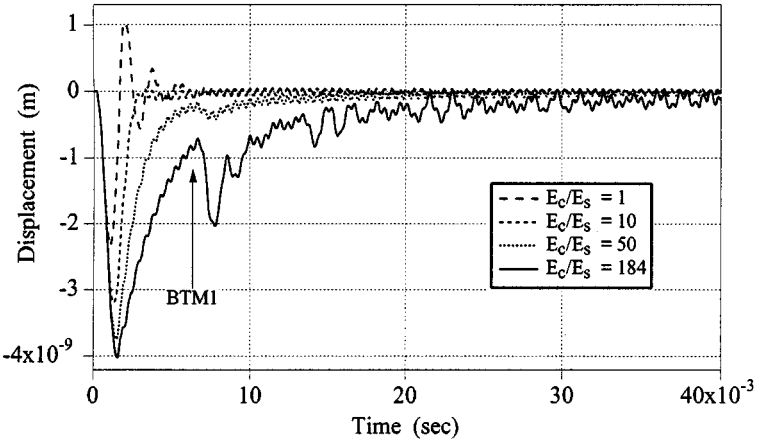

Figure 12. Displacement at top of pile with $H_T = 1$, $H_B = 11$, $k_E = E_c/E_s = 184$, 50, 10, and 1

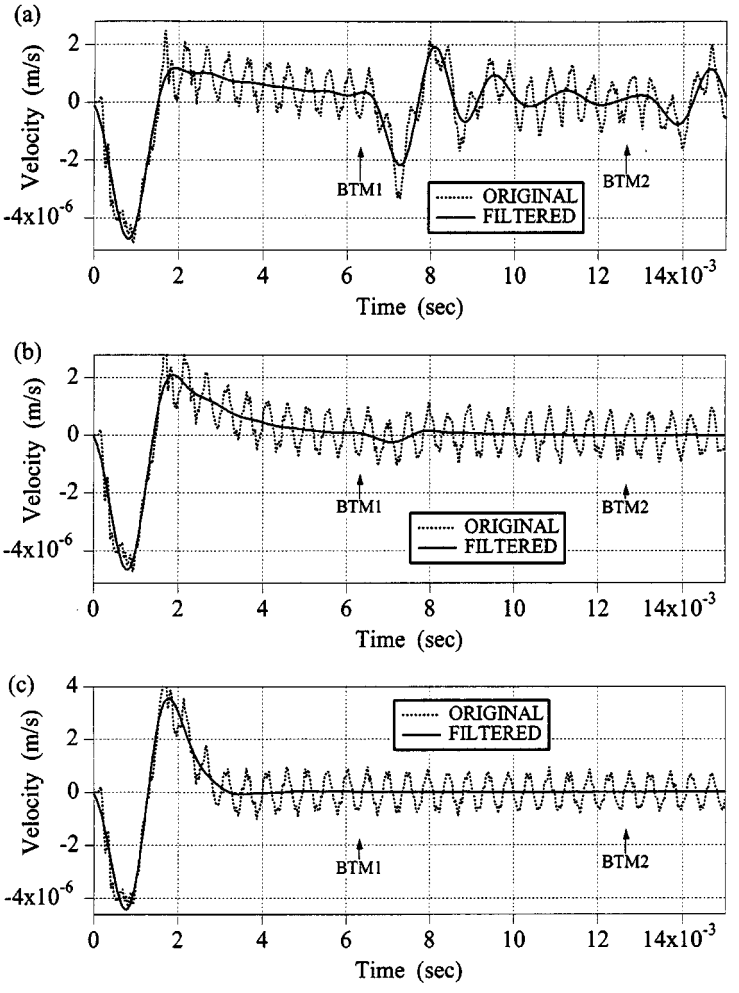

Figure 13. Original and filtered ($f_H = 1000$ Hz) velocities at top of pile with $H_T = 1$, $H_B = 11$, $E_c/E_s =$ (a) 184, (b) 50, and (c) 10

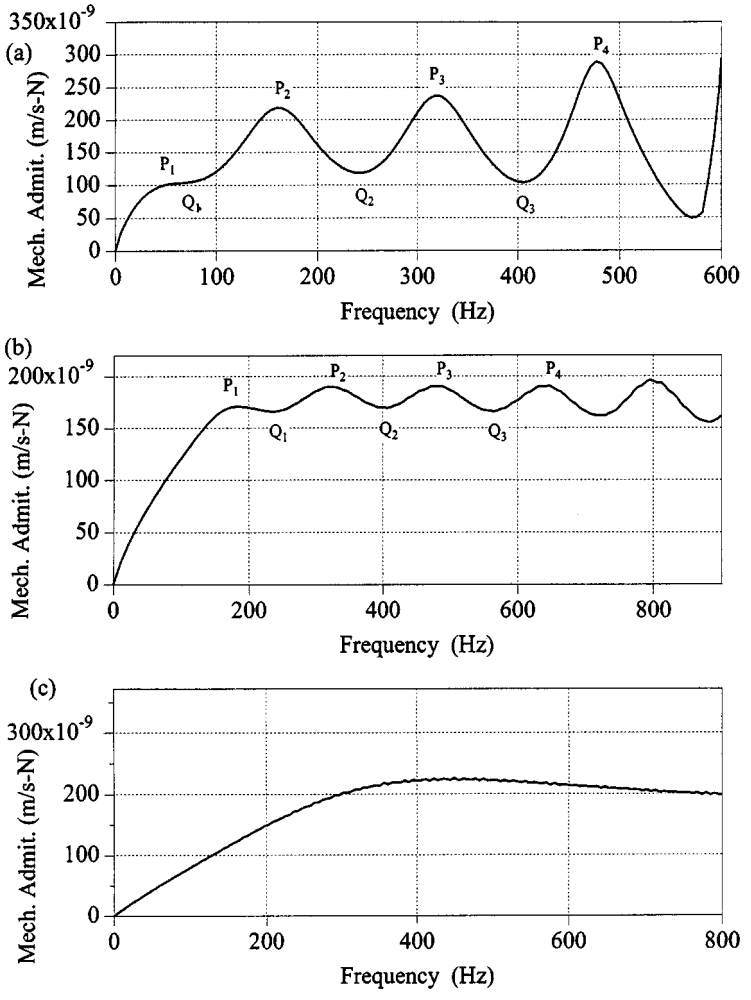

Figure 14. Mobility at top of pile with $H_T = 1$, $H_B = 11$, $E_c/E_s =$ (a) 184, (b) 50, and (c) 10

The mobilities of these three cases are plotted in Figure 14. The total length and the cross-sectional area of the pile are known to be $L = 12$ m and $A_c = \pi \times r_P^2 = 0.785$ m^2.

Equations (12) and (13) can be used to calculate the total length and the cross-sectional area of the pile. For the pile with $E_c/E_s = 184$ for example, the steady-state region may start at P_2 and end at P_4. Selecting this frequency interval to calculate the total length L and the minimum value at Q_2 and the maximum value at P_3 to obtain the cross-sectional area of the pile, A_c.

(1) $2\Delta f = f_{p4} - f_{p4} = 477{\cdot}3 - 159{\cdot}1 = 318{\cdot}2$(1/s),
(2) $L = V_{rod}/2\ \Delta f = 3790/318{\cdot}2 = 11.91$ m,
(3) error per cent $= (12 - 11{\cdot}91)/12 \times 100$ per cent $= 0{\cdot}75$ per cent,
(4) $R = \sqrt{(P_3 \times Q_2)} = \sqrt{(0{\cdot}2367 \times 0{\cdot}1181) \times 10^{-6}} = 0{\cdot}1672 \times 10^{-6}$ m/s N,
(5) $A_c = 1/(R\rho_c V_{rod}) = 1/(0{\cdot}1672 \times 10^{-6} \times 2300 \times 3790) = 0{\cdot}686$ m^2,
(6) error per cent $= (0{\cdot}785 - 0{\cdot}686)/0{\cdot}785 \times 100$ per cent $= 12{\cdot}6$ per cent.

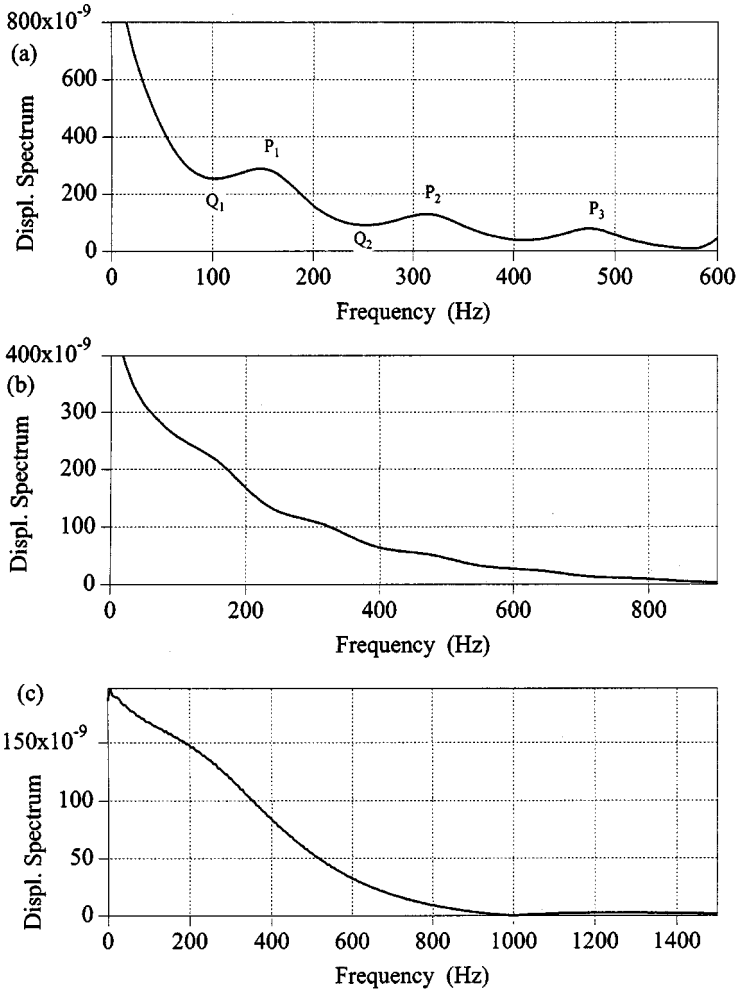

Figure 15. Displacement spectrum at pile head with $H_T = 1$, $H_B = 11$, $E_c/E_s =$ (a) 184, (b) 50, and (c) 10

Table II. Determination of length and cross-sectional area of pile with $H_T = 1$, $H_B = 11$ and $E_c/E_s = 184$ and 50 (f in 1/s, L in m, R in 10^{-6} m/s N, and A_c in m^2).

E_c/E_s	$2\Delta f = f_{p4} - f_{p2}$	L	error per cennt	$R = \sqrt{Q_2 P_3}$	A_c	error per cent
184	318·2	11·91	0·75	0·1672	0·686	12·6
50	329·2	11·51	4·08	0·1794	0·639	18·6

Similar calculations can be performed for the case with $E_c/E_s = 50$. The results are summarized in Table II. The process could not be applied however to the case with $k_E = 10$.

Figure 15 shows the displacement spectra used in the impact-echo method[9] for the three cases with $k_E = 184$, 50 and 10. The total length of the pile can then be calculated using Equation (14)

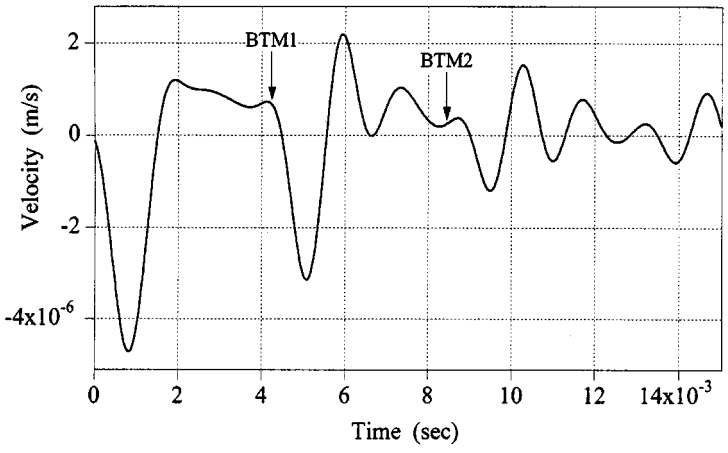

Figure 16. Velocity at top of pile with $H_T = 1$, $H_B = 7$ and $L/D = 8$

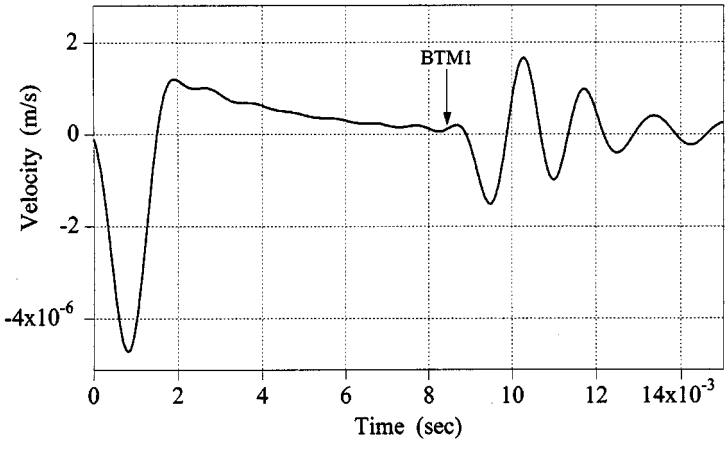

Figure 17. Velocity at top of pile with $H_T = 1$, $H_B = 15$ and $L/D = 16$

and the frequency f_1 associated with the first peak of the amplitude spectrum. For $E_c/E_s = 184$, $f_1 = 148{\cdot}1$ and thus $L = V_{rod}/2f_1 = 12{\cdot}8$ m. The error is 6·7 per cent. This process of analysis cannot be applied however to the other two cases because the peaks are very hard to identify.

4.3. Effect of pile length

Consider again the pile of Figure 2(b) where the length of the pile above ground is 1 m ($H_T = 1$ m). To evaluate the effect of the pile length which had been taken equal to 12 m in all the previous studies, the embedment depth was taken as 7, 15, 27, and 47 m representing total pile lengths of 8, 16, 28 and 48 m. The radius of the pile was kept constant $r_P = 0{\cdot}5$ m ($D = 2r_P = 1$ m). The theoretical times of arrival of the waves reflected from the bottom of the pile are marked with the characters 'BTM*n*'. The filtered velocity records at the pile top obtained from the 3-D models for pile lengths of 8, 16, 28 and 48 m are presented in Figures 16–19. It can be seen that the

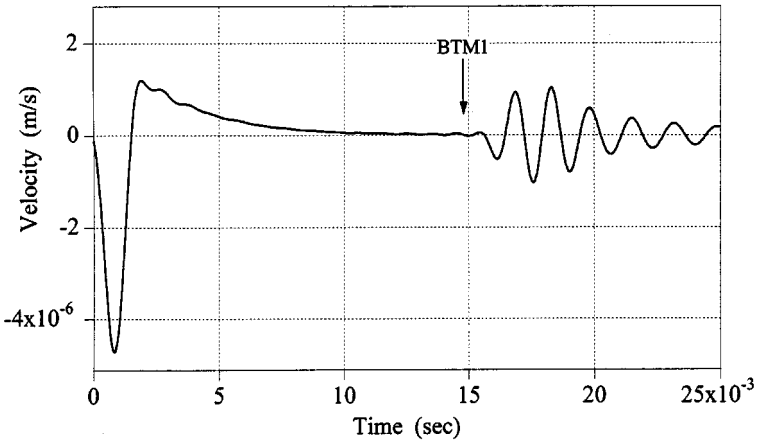

Figure 18. Velocity at top of pile with $H_T = 1$, $H_B = 27$ and $L/D = 28$

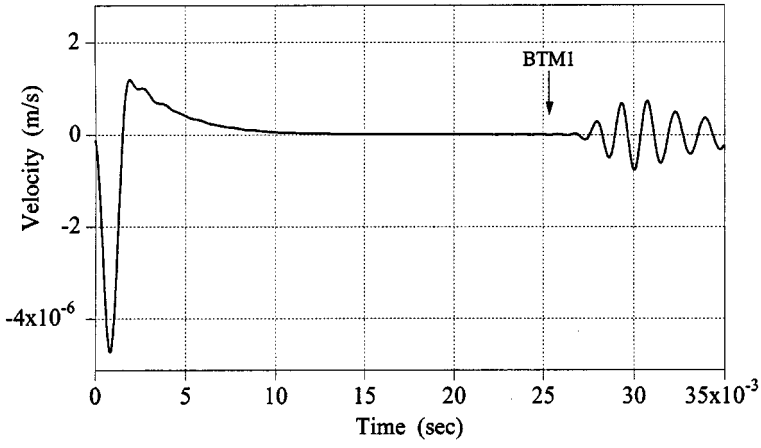

Figure 19. Velocity at top of pile with $H_T = 1$, $H_B = 47$ and $L/D = 48$

excursion corresponding to the arrival of the longitudinal wave reflected from the bottom of the pile becomes harder to identify as the length of the pile increases. The signal[26] associated with 'BTM1' is hardly identifiable once the length is larger than 20. This is so because the deeper the waves travel into the pile and soil, the larger the amount of energy dissipated into the soil. This finding is of practical significance in field tests, as mentioned by Davis:[4]

'Owing to the cumulative effect of soil damping on a long pile, a test in a pile of length/diameter ratio greater than 20 is unlikely to be very definite, …'

The corresponding mobilities are presented in Figures 20–23. Using equations (12) and (13), the predicted values of the total length and the cross-sectional area of the pile and the errors in the predictions are listed in Table III. The error in predicting the total length of the pile increases with the pile length but the error in the value of the cross-sectional area decreases. In all cases, the predictions of the length are very good (within 5 per cent).

The displacement spectra corresponding to the impact-echo method are shown in Figures 24–27. The predicted length of the pile for $L = 8$ is 8.2 m with an error of 2.5 per cent (first

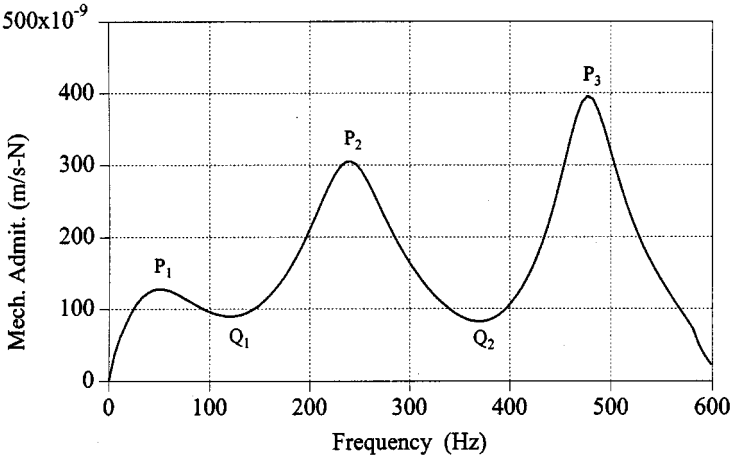

Figure 20. Mechanical admittance of pile with $H_T = 1$, $H_B = 7$ and $L/D = 8$

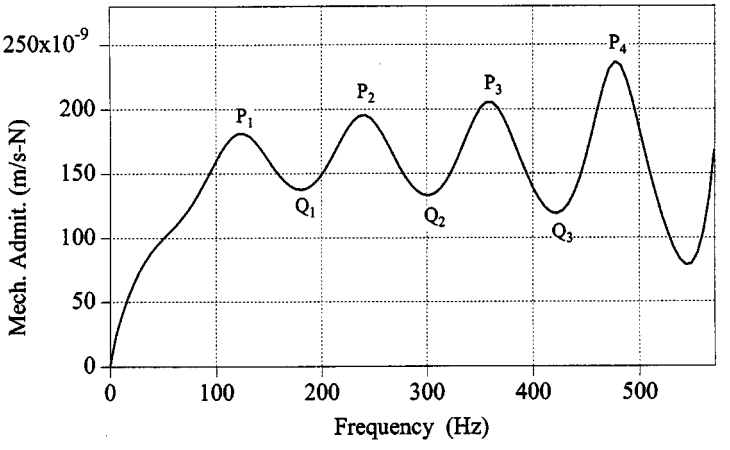

Figure 21. Mechanical admittance of pile with $H_T = 1$, $H_B = 15$ and $L/D = 16$

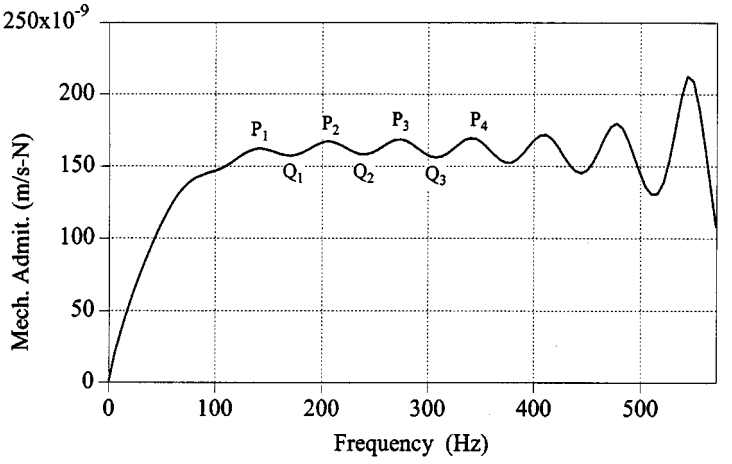

Figure 22. Mechanical admittance of pile with $H_T = 1$, $H_B = 27$ and $L/D = 28$

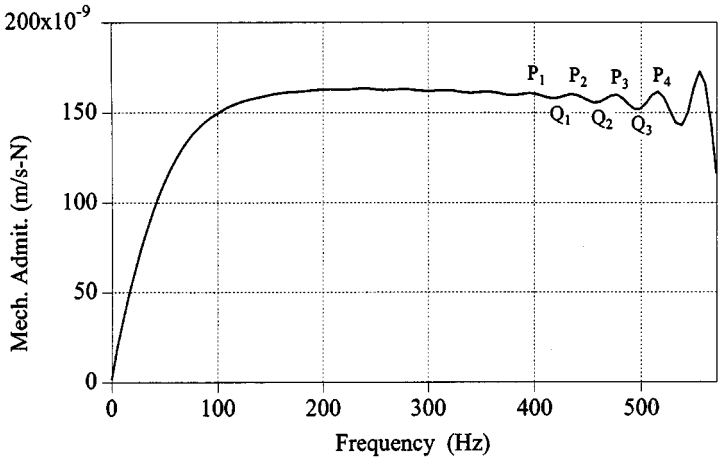

Figure 23. Mechanical admittance of pile with $H_T = 1$, $H_B = 47$ and $L/D = 48$

Table III. Determination of length and cross-sectional area of pile with $k_E = 184$, $H_T = 1$, $H_B = 7, 15, 27, 47$ and $L/D = 8, 16, 28, 48$ (f in 1/s, L in m, R in 10^{-6} m/s N, and A_c in m^2), using mobility method

L/D	$2\Delta f = f_{p4} - f_{p2}$	L	Error per cent	$R = \sqrt{(Q_2 P^3)}$	A_c	Error per cent
8	471·8	8·03	0·38	0·1806	0·635	19·1
16	235·9	16·07	0·44	0·1652	0·694	11·6
28	131·7	28·78	2·79	0·1634	0·702	10·6
48	82·3	46·05	4·06	0·1577	0·727	7·4

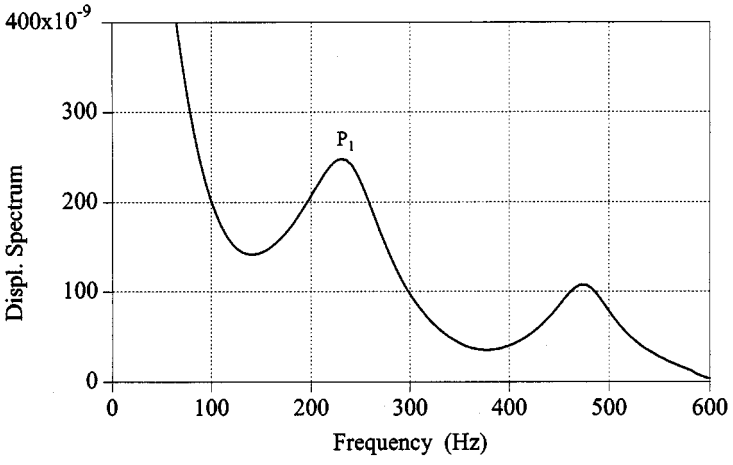

Figure 24. Displacement spectrum at pile head with $H_T = 1$, $H_B = 7$ and $L/D = 8$

frequency $f_1 = 230.4$ Hz). The first peak is harder to locate for $L = 16$ m but the following peaks can still be identified and the prediction of the length for this case would still be very reasonable. The location of the peaks and the prediction of the pile length for the cases $L = 28$ and 48 are, however, very difficult.

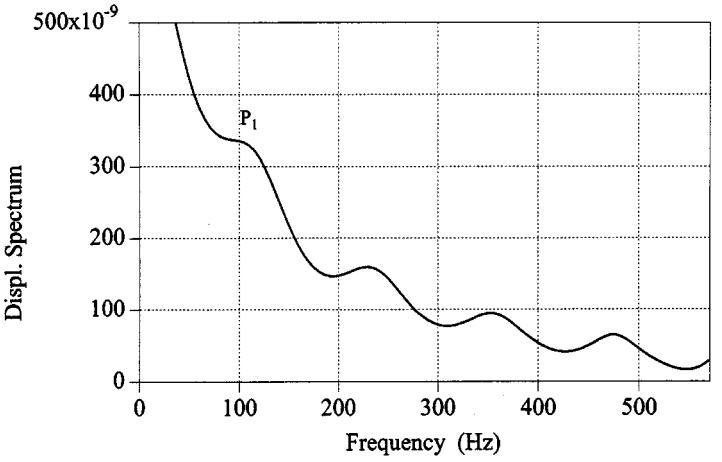

Figure 25. Displacement spectrum at pile head with $H_T = 1$, $H_B = 15$ and $L/D = 16$

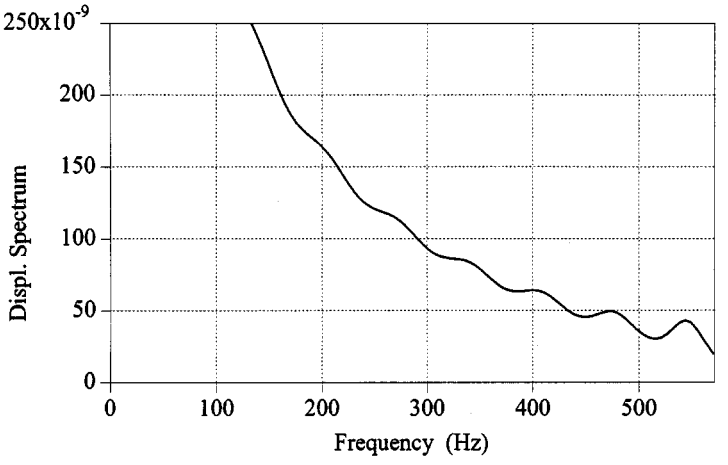

Figure 26. Displacement spectrum at pile head with $H_T = 1$, $H_B = 27$ and $L/D = 28$

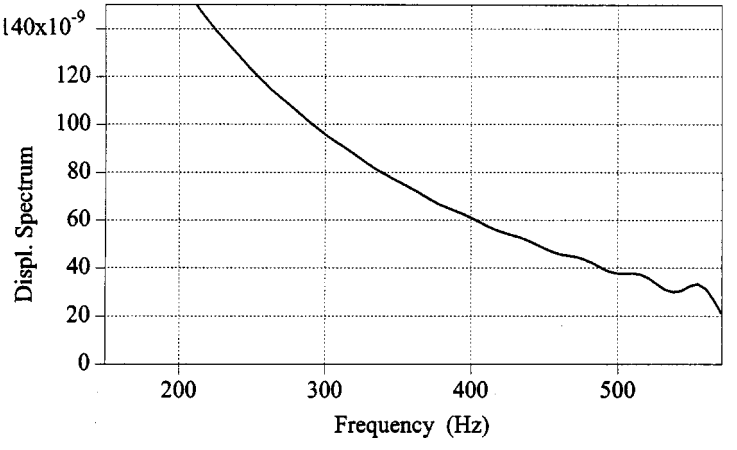

Figure 27. Displacement spectrum at pile head with $H_T = 1$, $H_B = 47$ and $L/D = 48$

5. CONCLUSIONS

The results of the studies conducted indicate that while the displacement records obtained with the 3-D model, which should be closer to those obtained in the field, are very similar in general terms to those predicted by the usual 1-D solutions, they exhibit some high-frequency oscillations which affect more strongly the velocity records and particularly the acceleration traces but have no useful significance for the problem under study. The use of high-frequency filters can help to eliminate these components and provide records which are more similar to the 1-D solutions and thus easier to interpret. The interpretation of the data to determine the pile length is, however, much easier using the mobility function in the frequency domain than working with the time records. The mobility function can provide very reasonable estimates not only of the pile length but also of the cross-sectional area and seems much more reliable than the simple displacement spectrum used in the impact echo method. However, for the method to work one needs a ratio of the Young's modulus of the pile to that of the surrounding soil of the order of 50 or larger and a length-to-diameter ratio of the pile of 30 or less.

REFERENCES

1. T. Whitaker, 'Structural integrity of piles', *Civil Eng*., 20–23 (1974).
2. J. Paquet, 'Etude vibratoire des pieux en beton; reponse harmonique', *Ann. Inst. Tech. Batim*., **21** (245), 789–803 (1968).
3. M. Briard, 'Controle des pieux par la methode des vibrations', *Ann. Inst. Tech. Batim*., **23** (270), 105–107 (1970).
4. A. G. Davis and C. S. Dunn, 'From theory to field experience with the non-destructive vibration testing of piles', *Proc. Instn Civil Eng*., Part 2, **57,** 571–593 (1974).
5. A. G. Davis and S. A. Robertson, 'Vibration testing of piles', *Struct. Eng*., **54** (6), A7–A10 (1976).
6. J. S. Higgs, 'Integrity testing of concrete piles by shock method', *Concrete*, **31**–**33** (1979).
7. R. T.Stain, 'Integrity testing', *Civil Eng*., London, 53–59 (1982).
8. R. T. Stain, 'Integrity testing,' *Civil Eng*., London, 71–73 (1982).
9. Y. Lin, M. Sansalone and N. J. Carino, 'Impact-echo response of concrete shafts', *Geotech. Test. J*., **14** (2), 121–137 (1991).
10. Y. Lin, M. Sansalone and N. J. Carino, 'Finite element studies of the impact-echo response of plates containing thin layers and voids', *J. Nondestr. Evaluation*, **9** (1) (1990).
11. M. Sansalone, and N. J. Carino, 'Transient impact response of thick circular plates', *NBS J. Res*., 355–367 (1987).
12. M. Sansalone, N. J. Carino and N. N. Hsu, 'A finite element study of transient wave propagation in plates', *NBS J. Res*., 267–278 (1987).
13. M. Sansalone, N. J. Carino and N. N. Hsu, 'A finite element study of the interaction of transient stress waves with planar flaws', *NBS J. Res*., 279–290 (1987).
14. M. Sansalone, N. J. Carino and N. N. Hsu, 'A finite element study of transient wave propagation in plates', *NBS J. Res*., 267–278 (1987).
15. M. Sansalone and N. J. Carino, 'Laboratory and field studies of the impact-echo method for flaw detection in concrete', a special publication by the American Concrete Institute on Nondestructive Testing of Concrete, *SP 112–1*, ACI, Detroit, MI, 1–20 (1988).
16. M. Sansalone and N. J. Carino, 'Impact-echo method', *Concr. Int*., 38–46 (1988).
17. Y. Lin and M. Sansalone, 'Detecting flaws in concrete beams and columns', *ACI Mater. J*., **89** (4), 394–405 (1992).
18. Y. Lin and M. Sansalone, 'Transient response of thick circular and square bars subjected to transverse elastic impact', *J. Acoust. Soc. Am*., **91** (2), 885–893 (1992).
19. Y. Lin and M. Sansalone, 'Transient response of thick rectangular bars subjected to transverse elastic impact', *J. Acoust. Soc. Am*., **91** (5), 2674–2685 (1992).
20. C. Cheng and M. Sansalone, 'The impact-echo response of concrete plates containing delaminations—numerical, experimental and field studies', *Mater. Struct*., **26** (159), 274–285 (1993).
21. J. -M. Lin and M. Sansalone, 'Impact-echo response of hollow cylindrical concrete structures surrounded by soil and rock: part I—numerical studies', *Geotech. Test. J*., **17** (2), 207–219 (1994).
22. J. -M. Lin and M. Sansalone, 'Impact-echo response of hollow cylindrical concrete structures surrounded by soil and rock: part II—experimental studies', *Geotech. Test. J*. **17** (2), 220–226 (1994).
23. A. J. G. Schellingerhout, 'Quantifying pile defects by integrity testing', *Application of Stress-Wave Theory to Piles, Int. Conf*., Balkema, Rotterdam, (1992), pp. 319–324.
24. J. O. Hallquist, 'User's manual for DYNA2D: an explicit two-dimensional hydrodynamic finite element code with interactive rezoning', *Report No. UCID-18756*, Lawrence Livermore National Laboratory, University of California, Livermore, CA, Rev. 2, 1984.

25. J. O. Hallquist, 'DYNA3D user's manual (nonlinear dynamic analysis of structures in three dimensions)', *Report No. UCID-19592,* Lawrence Livermore National Laboratory, University of California, Livermore, CA, Rev. 5, 1989.
26. S. T. Liao, 'Nondestructive testing of piles', *Ph.D. Dissertation*, University of Texas at Austin, 1994.
27. S. P. Timoshenko and J. N. Goodier, *Theory of Elasticity*, 3rd ed., McGraw-Hill, New York, 1970.
28. J. Lysmer and F. E. Richart, 'Dynamic response of footings to vertical loading', *J. Soil Mech. Found. Div. ASCE*, **92** (SM1), 65–91 (1966).
29. R. V. Whitman and F. E. Richart, 'Design procedures for dynamically loaded foundations', *J. Soil Mech. Found. Div. ASCE*, **93** (SM6), 169–193 (1967).
30. G. W. Blaney, E. Kausel and J. M. Roesset, 'Dynamic stiffness of piles', *Proc. 2nd Int. Conf. Numer. Methods in Geomech.*, Blacksburg, Virginia, 1976, pp. 1001–1012.
31. J. M. Roesset and D. Angelides, 'Dynamic stiffness of piles', in *Numerical Methods in Offshore Piling*, Institution of Civil Engineers, London, 1980, pp. 75–81.
32. J. M. Roesset, 'Stiffness and damping coefficients of foundations', in *Dynamic Response of Pile Foundations*, *Proc. Geotech. Eng. Div. ASCE*, 30 October 1980, pp. 1–30.

